

183464

ADAPTIVE TRACKING FOR COMPLEX SYSTEMS
USING REDUCED-ORDER MODELS

by

Craig R. Carignan
STX Corp.
Lanham, MD

Reduced-order models are considered in the context of parameter adaptive controllers for tracking workspace trajectories. A dual-arm manipulation task is used to illustrate the methodology and provide simulation results. A parameter adaptive controller is designed to track the desired position trajectory of a payload using a four-parameter model instead of a full-order, nine-parameter model. Several simulations with different payload-to-arm mass ratios are used to illustrate the capabilities of the reduced-order model in tracking the desired trajectory.

1.0 INTRODUCTION

Recent advances in control systems for robot manipulators have increased tracking accuracy far beyond the decoupled joint control schemes in predominant use a decade ago. Many controllers are based on computed torque schemes which use a model of the system to fabricate a feedforward portion to the control law in addition to an error feedback term. While the feedforward can mitigate the tracking error significantly, the reduction is strongly dependent upon the integrity of the model. Another important consideration is the additional computational burden imposed by a complex albeit accurate model.

Often, the model parameters are not known accurately because of the difficulty in measuring them or uncertainty about the object being manipulated. This difficulty can be overcome by using a "parameter adaptive controller" (see [1,2,3]) to update the model used by the control system. Depending upon the properties of the adaptation algorithm, the variable model can come very close to the true model and thus improve the tracking performance through the more accurate feedforward.

The algorithm developed in [3] has been found to be particularly successful in a number of applications including the MIT Whole Arm Manipulator [4] and, more recently, a Kraft Master Arm [5]. The latter application was a teleoperation experiment designed specifically to test the adaptation algorithm when the load on the arm was constantly changing due to the retrieval and release of payloads. The tracking capability of the adaptive controller was far superior to that of the PD controller with constant feedforward.

(NASA-CR-183464) ADAPTIVE TRACKING FOR
COMPLEX SYSTEMS USING REDUCED-ORDER MODELS
(ST Systems Corp.) 20 p CSCL 098

NPO-25609

Unclass

63/63 029223d

An interesting question arises when not only are the values of the model parameters uncertain but the validity of the model itself as well. This situation would occur, for example, when the equations of motion for a manipulator are divided into an arm/wrist decoupled model. Both the arm model and wrist model assume the other is fixed when determining the robot dynamics. Thus the arm link which is attached to the wrist is assumed to have fixed parameters in the arm model whereas, in actuality, the parameters are changing continuously due to wrist movement. The arm parameters cannot converge in this case because they are not really constant. Since the algorithm was designed assuming constant parameters, the question becomes, "Will the algorithm still work and, if so, how well?"

This question forms the theme for the remainder of this paper because it becomes a very important issue for more complex systems. Even in a system as simple as a single manipulator link, the inclusion of friction, backlash, drive train flexibility, sensor dynamics, etc. may become necessary to form a model accurate enough to have truly "constant" parameters. Pending the development of such a model, one could still be left with a model so complex that computation time starts to become an issue. Thus the use of a simple model may be propelled by the necessity of reducing on-line computations as well as off-line development.

This paper will address the issue of reduced-order models in the context of the parameter adaptive controller developed in [3]. The task studied will be the transport of a payload along a desired trajectory using two manipulator arms. The task will be studied in a plane to keep the demonstration simple while at the same time allowing significant departures of the reduced-order model from reality. The issue of how to incorporate a force distribution strategy for the two arms will also be addressed out of necessity due to the force redundancy present in the problem.

The report begins with a brief review of dual-arm dynamics with consideration given to kinematically redundant arms. A least squares torque strategy will be used for completely resolving the desired force trajectory for the arms and payload. A parameter adaptive controller will then be designed to track the desired position trajectory of the payload using a reduced-order model for the arm/payload dynamics. Several simulations using different payload-to-arm mass ratios will be used to illustrate the capabilities of the reduced-order model in replicating the dynamics of the actual system.

2.0 TRANSPORT DYNAMICS

The dual-arm robot configuration is depicted in Fig. 1. The relative joint angles for arms A and B are $\mathbf{q}_a^T = [\theta_{1a} \theta_{2a} \theta_{3a}]$ and $\mathbf{q}_b^T = [\theta_{1b} \theta_{2b} \theta_{3b}]$ (positive angles are counterclockwise). The base of arm A is at point (x_{oa}, y_{oa}) and arm B at (x_{ob}, y_{ob}) . The length, mass, inertia and center of mass of link i are l_i , m_i , I_i and x_{cmi} respectively. The link 1 and 2 center of mass and inertia are referenced to the attach point with the subsequent link (x_{cmi} is negative). Link 3's center of

mass is assumed to be at the attach point to the payload, and as with the inertia I_3 , is measured from the wrist joint and has positive value I_3 .

The inertial coordinates for the payload are $\underline{x}_e^T = [x_e \ y_e \ \theta_e]$. The payload has mass m_e , length $2l_e$ (with x_e and y_e at the midpoint), and inertia I_e about its geometric center. The center of mass is at position (x_{cme}, y_{cme}) with respect to the payload's body coordinates which parallel the reference coordinates when $\theta_e=0$.

The free-body diagram of Fig. 2 assists in the generation of the system dynamics. The payload exerts a force f_a and f_b on arms A and B, respectively, and thus has a reaction force exerted on it of $-f_a$ and $-f_b$ if the connection is rigid. Thus the arm dynamics are given by

$$\begin{bmatrix} M_a & 0 \\ 0 & M_b \end{bmatrix} \begin{bmatrix} \ddot{q}_a \\ \ddot{q}_b \end{bmatrix} + \begin{bmatrix} g_a \\ g_b \end{bmatrix} = \begin{bmatrix} I_a \\ I_b \end{bmatrix} + \begin{bmatrix} J_a^T f_a \\ J_b^T f_b \end{bmatrix} \quad (1)$$

and payload dynamics by

$$M_e \ddot{x}_e + g_e = -J_{ea}^T f_a - J_{eb}^T f_b \quad (2)$$

M_i is commonly called the "mass matrix" and g_i is a nonlinear vector characterized by Coriolis and centripetal force terms. I_a and I_b are the torques exerted at the arm joints, and f_a and f_b are the beam interaction forces described above. The J_i are known as "Jacobians" and convert the forces at the end effector into arm torques. These equations are presented in full in Appendix A.

In addition to these dynamical equations, there are also equations of constraint due to the connection of the arms through the payload

$$\begin{aligned} x_e &= h_a(q_a) \\ x_e &= h_b(q_b) \end{aligned} \quad (3)$$

which are given in Appendix A. The constraints (3) can be differentiated and combined with the system equations through a procedure called the "reduction transformation" (see [6]) to eliminate the interaction forces f_a and f_b . The procedure for this particular example can be found in [7] and the results are

$$\begin{bmatrix} J_{ea}^{-1} Q_a^{-1} + M_e^{-1} J_{ea}^T & M_e^{-1} J_{eb}^T \\ M_e^{-1} J_{ea} & J_{eb}^{-1} Q_b^{-1} + M_e^{-1} J_{eb}^T \end{bmatrix} \begin{bmatrix} f_a \\ f_b \end{bmatrix} = \begin{bmatrix} -D_a M_a^{-1} I_a + D_a M_a^{-1} g_a - M_e^{-1} g_e - D_a \dot{g}_a \\ -D_b M_b^{-1} I_b + D_b M_b^{-1} g_b - M_e^{-1} g_e - D_b \dot{g}_b \end{bmatrix} \quad (4)$$

where

$$D_a \equiv J_{ea}^{-1} J_a \quad Q_a^{-1} = J_a M_a^{-1} J_a^T \quad (5)$$

$$D_b \equiv J_{eb}^{-1} J_b \quad Q_b^{-1} = J_b M_b^{-1} J_b^T$$

The interaction forces can now be solved in terms of the arm torques using the reduced dynamics (4) and payload dynamics (2). Solving for f_b from (2) gives

$$f_b = -J_{eb}^T [J_{ea} f_a + M_e \ddot{x}_e + g_e] \quad (6)$$

Substituting (6) into (4), premultiplying the arm A partition by J_{ea} , and then solving for f_a yields

$$f_a = Q_a [-J_a M_a^{-1} I_a + J_e \ddot{x}_e + J_a M_a^{-1} g_a - J_e \dot{d}_a \dot{q}_a] \quad (7)$$

Using a parallel procedure, the arm B interaction forces are

$$f_b = Q_b [-J_b M_b^{-1} I_b + J_{eb} \ddot{x}_e + J_b M_b^{-1} \dot{q}_b - J_{eb} \dot{D}_b \dot{q}_b] \quad (8)$$

Substituting (7) and (8) into (2) and regrouping terms gives

$$\begin{array}{c} \text{arm A} \\ \Downarrow \\ J_{ea}^T Q_a J_a M_a^{-1} I_a + J_{eb}^T Q_b J_b M_b^{-1} I_b = [\quad J_{ea}^T Q_a J_{ea} + J_{eb}^T Q_b J_{eb} + M_e] \ddot{x}_e \\ + J_{ea}^T Q_a J_a M_a^{-1} \ddot{q}_a + J_{eb}^T Q_b J_b M_b^{-1} \ddot{q}_b + \ddot{q}_e \\ - J_{ea}^T Q_a J_{ea} \dot{D}_a \dot{q}_a - J_{eb}^T Q_b J_{eb} \dot{D}_b \dot{q}_b \end{array} \quad (9)$$

Equation (9) represents the equation of motion of the arm/payload system in payload coordinates. The terms in brackets represent the inertial forces needed to accelerate the arms and payload along the desired trajectory; the "Q" terms are the inertia tensors for the arms projected onto the end-effector, and " J_e " is an additional transformation to the payload origin. The \mathbf{g} terms represent Coriolis and centripetal forces in joint coordinates, and the joint velocity terms result from the time varying nature of the arm jacobians when transforming joint velocities into end-effector velocities.

Since (9) only contains one acceleration term, (9) can be solved for \ddot{x}_e if the term in brackets is invertible. The arm interaction forces are obtained by substituting \ddot{x}_e into (7) and (8). The interaction forces can then be substituted into the equations of motion for the two arms (1) to give the joint accelerations.

3.0 CONTROL SYSTEM

The matrix "Q" defined in (5) has appeared previously in the literature in the context of impedance control. In [8], Q is referred to as the "end-point mobility tensor" as opposed to the "mobility tensor" which is the manipulator's inverse inertia matrix. By generating the kinetic energy quadratic with the momentum

vector in end-effector coordinates, the resulting surfaces of constant energy form "ellipsoids of gyration" in the momentum space. The shape and orientation of the ellipsoid indicate how much inertial resistance there is to motion in a particular direction, hence the term "mobility."

The concept of mobility tensors is a useful insight for forming a reduced order model for the dual-arm system. The term in brackets in (9) can be considered a superposition of the mobility tensors of the payload and the two arms, all contributing to the mobility of the arm/payload system from the perspective of the payload's position. Is it possible that if the arm terms are ignored but the parameters in the payload's mobility tensor are allowed to vary, that the model can absorb the effect of the arm mobility tensors as well? In addition, since the Coriolis and centripetal forces result from the time variation of the inertia tensor, can the remaining terms in (9) be effectively accounted for through the time variation of the payload parameters?

The idea of superposition provides the underlying basis for using the following equation for a model of the actual system dynamics in (9):

$$\hat{M}_e \ddot{x}_e + \hat{C}_e \dot{x}_e = \hat{f}_e \quad (10)$$

\hat{M}_e and \hat{C}_e are the same as M_e and C_e given in Appendix A except they depend upon the model parameters $\hat{\rho}_e$ instead of the payload parameters ρ_e . The quantity \hat{f}_e is the modeled total force applied to the arm/payload system and is given by

$$\hat{f}_e = A^T I_a + B^T I_b \quad (11)$$

$$\text{where } A^T \equiv J_{ea}^{TA} Q_a J_a \hat{M}_a^{-1}$$

$$B^T \equiv J_{eb}^{TB} Q_b J_b \hat{M}_b^{-1}$$

If the arm inertia tensors are known precisely, (11) reduces to the left side of (9), constituting an exact relationship between the arm torques and system force f_e . Deviations from the actual inertia tensors generate additional errors which must be absorbed by the model parameters.

The control law is formulated from the adaptive algorithm in [3] and is given by

$$f_{ec} = \hat{M}_e (\ddot{x}_{er} - \lambda \underline{s}) + \hat{C}_e \dot{x}_{er} \quad (12)$$

$$\dot{x}_{er} = \dot{x}_{ed} - \lambda \tilde{x}_e$$

$$\tilde{x}_e = \underline{x}_e - \dot{\underline{x}}_e$$

$$\underline{s} = \underline{x}_e + \lambda \dot{\underline{x}}_e$$

The parameter adaptation law is

$$\dot{\hat{p}}_e = -\Gamma^{-1} Y_e^T \hat{s} \quad (13)$$

where Γ is a diagonal matrix of positive constant gains and Y_e is the parameter coefficient matrix given in Appendix B.

The control law in (12) only specifies the total force to be applied to the payload; it is not a control law for the arms. Since either arm alone can deliver the requisite force, the force redundancy must be resolved via some artificial constraint imposition. The next section will present one way of effecting the desired force on the payload using both arms.

4.0 FORCE RESOLUTION

Given that the system force in (11) is specified by (12), the task now at hand is to determine the arm torques, τ_a and τ_b . Since the three degrees of planar motion of the payload through the workspace are governed by f_e , there is an excess of three arm torques available to achieve this motion. Thus the arm torques can be anything as long as the three constraints in (11) hold.

One approach to determining a unique solution is to optimize some cost criterion while adjoining any existing constraints on variables being optimized. A natural choice is to minimize the amount of current drawn by the arm motors, especially if the motors are being powered by on-board batteries. Since torque is proportional to current in a d-c motor, the energy used will also be proportional to the torque.

A measure of the quantity of torque used might be the mean square cost

$$C = \frac{1}{2} \tau_a^T \tau_a + \frac{1}{2} \tau_b^T \tau_b \quad (14)$$

Though this cost is not an exact reflection of the power being drawn by the motors, its advantage over other measures is that it leads to an analytical solution. If the constraint in (11) for $\hat{f}_e = f_{ec}$ is adjoined to the cost using a Lagrange multiplier, and the resulting Hamiltonian is minimized with respect to the arm torques, the "optimum" arm torques become

$$\begin{aligned} \tau_a &= A(A^T A + B^T B)^{-1} f_{ec} \\ \tau_b &= B(A^T A + B^T B)^{-1} f_{ec} \end{aligned} \quad (15)$$

Thus (15) together with (12) constitutes the control law for the torques to be applied to the two arms.

The relationship in (15) is a more general result than the one found in [7,9] because it does not assume that the arm and payload dimensionality are the same. If the arms are not redundant, A and B are square and a direct relationship between the torques in the two arms can be found using (15). In addition, if the arm jacobians are invertible, the inertia tensors cancel out and the relationship becomes completely geometric, involving only jacobians.

5.0 SIMULATIONS

A number of simulations were performed between the initial and final configurations shown in Figure 3. The initial payload position was $x_e^T = [0.60 \ 0.20 \ 0.35]$ and the final position was $x_e^T = [0.80 \ -0.20 \ -0.35]$. The corresponding link parameters for the arms were the same and are given in Table 1. The baseline parameters for the payload were $m_e = 1.0$ kg, $i_e = 0.2$ kg-m², and $x_{cme} = y_{cme} = 0.0$ m. The arm bases were equidistantly spaced 0.5 m from the reference x-axis, and the grippers were equidistantly spaced 0.5 m from the payload x-axis.

Table 1: Arm parameters used in simulations.

link #	length (m)	mass (kg)	c.m. (m)	inertia (kg-m ²)
1	0.5	1.0	-0.25	0.05
2	0.5	1.0	-0.25	0.05
3	0.1	0.2	0.10	0.01

The desired trajectory for the payload consisted of a constant acceleration followed by a constant deceleration phase of the same magnitude for each coordinate. The total time for each test was 5.0 sec, and the control bandwidth was $\lambda = 5.0$ rad/sec. The adaptation gain matrix for the baseline case was $\Gamma = \text{diag}(0.001, 0.005, 0.001, 0.001)$. The parameters in the control model were initialized to be the same as the payload parameters. The arm parameters and configuration geometry were all assumed to be known precisely.

The tracking algorithm was simulated for three different ratios of payload mass to link mass: (a) 1:5, (b) 1:1 and (c) 5:1 (inertia ratios were also the same). A ratio of 1:5 represents the most severe test of the algorithm where the arm masses and inertias dominate the system dynamics, whereas a ratio of 5:1 represents the case closest to the model used by the control system. Equal payload and link masses represent the baseline case.

The diagonal elements of the modeled mass matrix are plotted in Figure 4 for the three different payload/link ratios. These elements are normalized by the corresponding elements of the actual system mass matrix M (the coefficient of \ddot{x}_e in (9)): $\rho^T = [p_{e1}/M_{11} \ p_{e1}/M_{22} \ p_{e2}/M_{33}]$. For large payload/link masses, the normalized parameters should approach unity since the system mass is

dominated by the payload, and the control model is based on the dynamics of a single rigid body. As the arm masses start to become a factor, however, the p_i can deviate significantly since a degenerate model is being used to replicate the system dynamics. Even for dominant payloads, however, the parameters are not guaranteed to converge unless the trajectory is sufficiently rich to excite all the dynamics affected by the parameters.

The convergence time also depends strongly upon the adaptation gains. The adaptation gains in the baseline case were selected to give rise times on the order of 1 sec but not so high as to produce large overshoots. Since larger parameters required faster adaptation, the gains were increased by a factor of ten for the high payload/link ratio and decreased by a factor of ten for the low payload/link mass ratio.

The normalized parameters undergo their closest approach to unity in the 5:1 case of Fig. 4c midway through the trajectory when the payload speed was highest. The normalized inertia, p_3 , is the most unstable of the three parameters because of its relatively small size. The oscillatory behavior in the first half of the trajectory could be eliminated by choosing a smaller adaptation gain for the inertia. As the payload slows down, the trajectory is no longer "persistently exciting" enough to keep the parameters on track. The 1:5 case exhibits the worst behavior, with large overshoots and incomplete parameter convergence.

Though the parameter convergence is a good indicator of how well the tracking algorithm is working, the goal of the control system is to minimize the tracking errors, s_i . The tracking errors for the two cartesian positions of the payload, x_e and y_e , and orientation, q_e , are shown in Figures 5-7 both with and without parameter adaptation. In the nonadaptive cases, the parameters were held constant at the value of the payload parameters.

The tracking errors display similar characteristics over the evolution of the trajectory. For most cases, the errors for the adaptive cases start out almost as large as the nonadaptive errors. Once the parameters have had a chance to adapt (around 1 sec), the errors take a rather sharp drop which is usually maintained through the remainder of the trajectory. Sometimes the errors decrease as the payload comes to a stop due to the divergent behavior of the parameters when the velocities go to zero.

All three payload/link ratios showed significant reductions in tracking errors for the adaptive runs over the nonadaptive runs. Even the 5:1 case with the payload dominating the dynamics showed reductions on the same order as the case where the arm masses dominate. Thus it is not clear that by choosing constant parameters based on the system mass matrix rather than the payload parameters, the tracking errors would have been reduced significantly for the 1:5 case.

6.0 CONCLUSIONS

This report has explored one option for improving tracking performance without resorting to higher control bandwidths. The approach used was to implement an adaptive controller modeled upon a much simpler system than that which was actually present. Though the use of a reduced-order model negated any prospects for the parameters to converge, it was hoped the model would provide an accurate enough feedforward to improve the tracking performance significantly over constant gain methods.

What was discovered was encouraging. The adaptive controller was able to reduce tracking errors substantially over the constant gain approach even for cases where the payload began to dominate the system dynamics. This meant that even when only slight perturbations to the four-parameter model used by the controller were present, the adaptive controller could reduce the tracking errors significantly, as if a full-order model were being used. Thus even a crude model like the one used here could offer significant improvement over nonadaptive methods.

Much work remains to be done on the use of reduced-order models for tracking control. Though a simple dual arm system has been tested in some detail, there are many other applications which could benefit from using the same approach. In particular, the segmentation of a manipulator arm into two decoupled models for the controller is one area currently under investigation. A full three-dimensional dual-arm task is also being considered. It is hoped that reducing the order of the model used by the controller will allow the use of adaptive control in manipulation tasks once thought too computationally intensive for model-based control.

ACKNOWLEDGEMENTS

This research was sponsored by NASA Goddard Space Flight Center under contract # 28561.

REFERENCES

1. Khosla, P., "Parameter Identification of Robot Dynamics," Proc. 24th Conf. on Decision and Control, pp. 1754-1760, December 1985
2. Craig, J., Hsu, P., and Sastry, S., "Adaptive Control of Mechanical Manipulators," Proc. IEEE Conf. on Robotics and Automation, pp. 190-195, San Francisco, 1986
3. Slotine, J-J., and Li, W., "On the Adaptive Control of Robot Manipulators," Int. J. Robotics Research, Vol. 6, No. 3, 1987

4. Niemeyer, G., and Slotine, J-J., "Computational Algorithms for Adaptive Compliant Motion," Proc. IEEE Conf. on Robotics and Automation, pp. 566-571, Scottsdale, Arizona, May 1989
5. Carignan, C., Tarrant, J., and Mosier, G., "Adaptive Control for Improving Operator Performance during Teleoperation," Proc. IEEE Conf. on Systems, Man and Cybernetics, Cambridge, Mass. 1989
6. McClamroch, N., "Singular Systems of Differential Equations as Dynamic Models for Constrained Robot Systems," Proc. IEEE Conf. on Robotics and Automation, pp. 21-28, San Francisco, 1986
7. Carignan, C., and Akin, D., "Optimal Force Distribution for Payload Positioning Using a Planar Dual-Arm Robot," J. Dynamic Systems, Measurement, and Control, Vol. 111, June 1989
8. Hogan, N., "Impedance Control of Industrial Robots," Robotics and Computer-Integrated Manufacturing, Vol. 1, No. 1, pp. 97-113, 1984
9. Carignan, C., and Akin, D., "Cooperative Control of Two Arms in the Transport of an Inertial Load in Zero Gravity," J. Robotics and Automation, Vol. 4, No. 4, August 1988

APPENDIX A: SYSTEM EQUATIONS OF MOTION

payload equations of motion:

$$M_e \ddot{x}_e + g_e = f_e$$

$$M_e = \begin{bmatrix} p_{e1} & 0 & -p_{e3}s_e - p_{e4}c_e \\ 0 & p_{e1} & p_{e3}c_e - p_{e4}s_e \\ -p_{e3}s_e - p_{e4}c_e & p_{e3}c_e - p_{e4}s_e & p_{e2} \end{bmatrix}$$

$$g_e = \begin{bmatrix} (-p_{e3}c_e + p_{e4}s_e)\theta_e^2 \\ (-p_{e3}s_e - p_{e4}c_e)\theta_e^2 \\ 0 \end{bmatrix} = C_e \dot{x}_e \quad C_e = \begin{bmatrix} 0 & 0 & (-p_{e3}c_e + p_{e4}s_e)\theta_e \\ 0 & 0 & (-p_{e3}s_e - p_{e4}c_e)\theta_e \\ 0 & 0 & 0 \end{bmatrix}$$

$$\dot{x}_e = \begin{bmatrix} x_e \\ y_e \\ \theta_e \end{bmatrix}$$

$$\ddot{x}_e = \begin{bmatrix} m_e \\ i_e \\ m_e x_{cm} \\ m_e y_{cm} \end{bmatrix}$$

$$s_e \equiv \sin \theta_e$$

$$c_e \equiv \cos \theta_e$$

arm equations of motion:

$$M \ddot{q} + g = \tau + J^T f$$

$$M = \begin{bmatrix} p_1 + 2l_1p_4c_2 + 2l_2p_5c_3 + 2l_1p_5c_3 & p_2 + l_1p_4c_2 + 2l_2p_5c_3 + l_1p_5c_{23} & p_3 + l_2p_5c_3 + l_1p_5c_{23} \\ p_2 + l_1p_4c_2 + 2l_2p_5c_3 + l_1p_5c_{23} & p_2 + 2l_2p_5c_3 & p_3 + l_2p_5c_3 \\ p_3 + l_2p_5c_3 + l_1p_5c_{23} & p_3 + l_2p_5c_3 & p_3 \end{bmatrix}$$

$$C = \begin{bmatrix} l_1(p_4s_2 + p_5s_{23}) & l_2p_5s_3 - l_1p_4s_2 & -p_5(l_2s_3 + l_1s_{23}) \\ l_1(p_4s_2 + p_5s_{23}) & l_2p_5s_3 & -l_2p_5s_3 \\ l_1p_5s_{23} & l_2p_5s_3 & 0 \end{bmatrix} \quad \dot{\theta}^2 = \begin{bmatrix} \dot{\theta}_1^2 \\ (\dot{\theta}_1 + \dot{\theta}_2)^2 \\ (\dot{\theta}_1 + \dot{\theta}_2 + \dot{\theta}_3)^2 \end{bmatrix}$$

$$g = C \dot{\theta}^2$$

$$\ddot{q} = \begin{bmatrix} \theta_1 \\ \theta_2 \\ \theta_3 \end{bmatrix}$$

$$\underline{\Omega} = \begin{bmatrix} i_1 + i_2 + i_3 + l_1^2(m_1 + m_2 + m_3) + 2l_1m_1x_{cm1} + l_2^2(m_2 + m_3) + 2l_2m_2x_{cm2} \\ i_2 + i_3 + l_2^2(m_2 + m_3) + 2l_2m_2x_{cm2} \\ i_3 \\ m_2x_{cm2} + l_2(m_2 + m_3) \\ m_3x_{cm3} \end{bmatrix}$$

$$s_{ij} \equiv \sin(q_i + q_j)$$

$$c_{ij} \equiv \cos(q_i + q_j)$$

constraint equations:

$$x_{eff} = l_1 c_1 + l_2 c_{12} + l_3 c_{123} + x_0$$

$$y_{eff} = l_1 s_1 + l_2 s_{12} + l_3 s_{123} + y_0$$

$$\theta_{eff} = q_1 + q_2 + q_3$$

$$J = \frac{\partial \underline{x}_{eff}}{\partial \underline{q}} = \begin{bmatrix} -l_1 s_1 - l_2 s_{12} - l_3 s_{123} & -l_2 s_{12} - l_3 s_{123} & -l_3 s_{123} \\ l_1 c_1 + l_2 c_{12} + l_3 c_{123} & l_2 c_{12} + l_3 c_{123} & l_3 c_{123} \\ 1 & 1 & 1 \end{bmatrix}$$

$$x_e = x_{eff} + \begin{cases} l_e s_e & \text{arm A} \\ -l_e s_e & \text{arm B} \end{cases}$$

$$y_e = y_{eff} + \begin{cases} -l_e c_e & \text{arm A} \\ l_e c_e & \text{arm B} \end{cases}$$

$$\theta_e = \theta_{eff}$$

$$J_e = \frac{\partial \underline{x}_{eff}}{\partial \underline{x}_e}$$

$$J_{ea} = \begin{bmatrix} 1 & 0 & l_e c_e \\ 0 & 1 & l_e s_e \\ 0 & 0 & 1 \end{bmatrix}$$

$$J_{eb} = \begin{bmatrix} 1 & 0 & -l_e c_e \\ 0 & 1 & -l_e s_e \\ 0 & 0 & 1 \end{bmatrix}$$

APPENDIX B: PARAMETER UPDATE DYNAMICS

parameter adaptation law:

$$\dot{\hat{\rho}}_e = -\Gamma^{-1} Y_e^T \underline{s}$$

$$\text{where } \dot{\hat{\rho}}_e (\hat{\rho}_e - \rho_e) = (\hat{M}_e - M_e) [\ddot{x}_{er} - \lambda s] + (\hat{C}_e - C_e) \dot{x}_{er}$$

$$Y_e^T = \begin{bmatrix} \ddot{x}_{er1} - \lambda s_1 & \ddot{x}_{er2} - \lambda s_2 & 0 \\ 0 & 0 & \ddot{x}_{er3} - \lambda s_3 \\ -s_e(\ddot{x}_{er3} - \lambda s_3) - c_e \dot{x}_{er3}^2 & c_e(\ddot{x}_{er3} - \lambda s_3) - s_e \dot{x}_{er3}^2 & -s_e(\ddot{x}_{er1} - \lambda s_1) + c_e(\ddot{x}_{er2} - \lambda s_2) \\ -c_e(\ddot{x}_{er3} - \lambda s_3) + s_e \dot{x}_{er3}^2 & -s_e(\ddot{x}_{er3} - \lambda s_3) - c_e \dot{x}_{er3}^2 & -c_e(\ddot{x}_{er1} - \lambda s_1) - s_e(\ddot{x}_{er2} - \lambda s_2) \end{bmatrix}$$

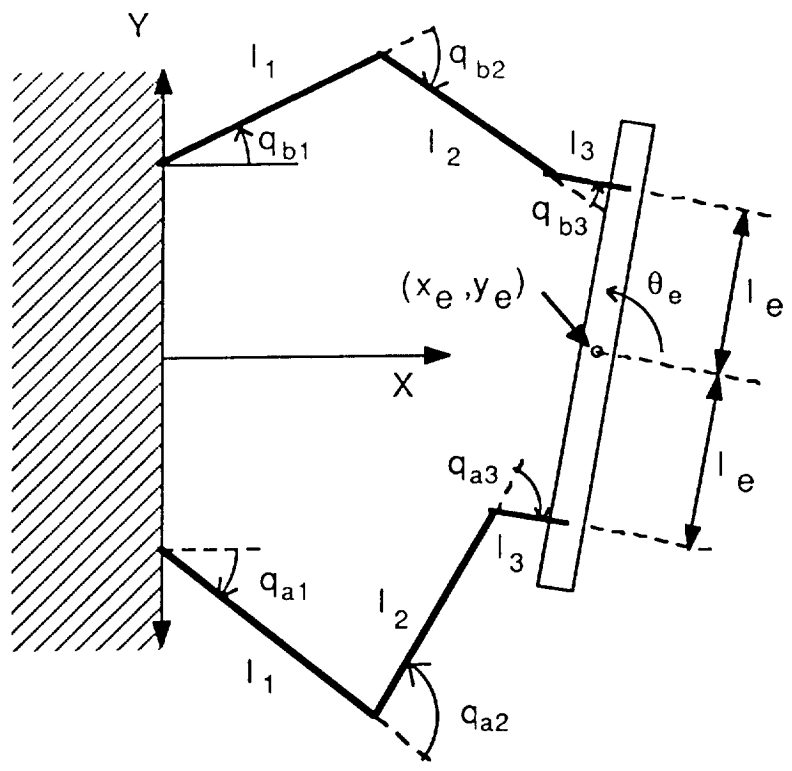


Figure 1: Two-arm geometry and coordinates.

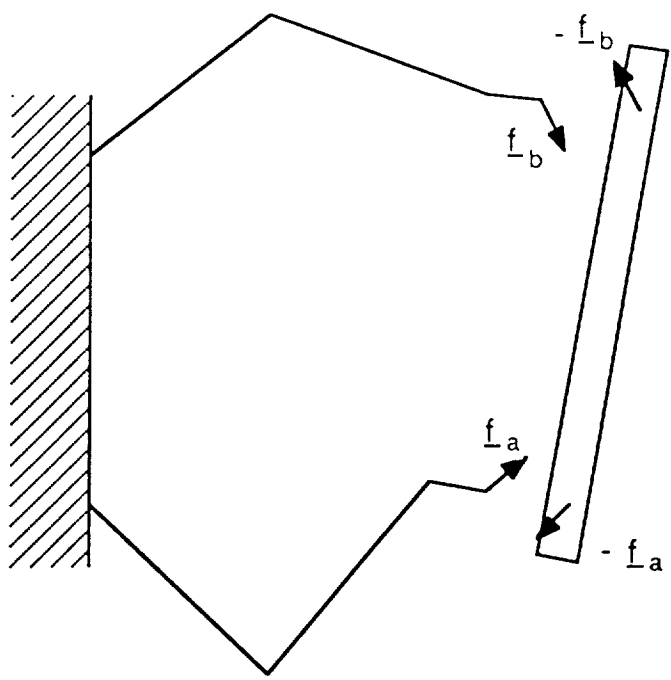
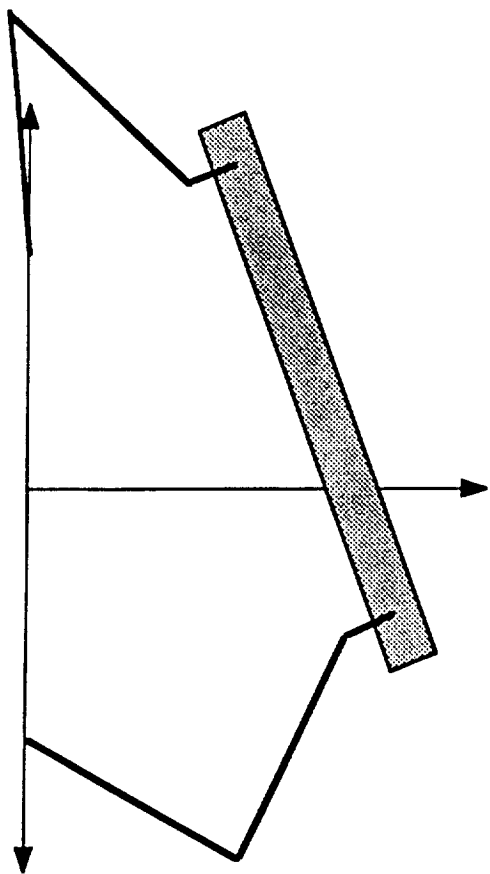
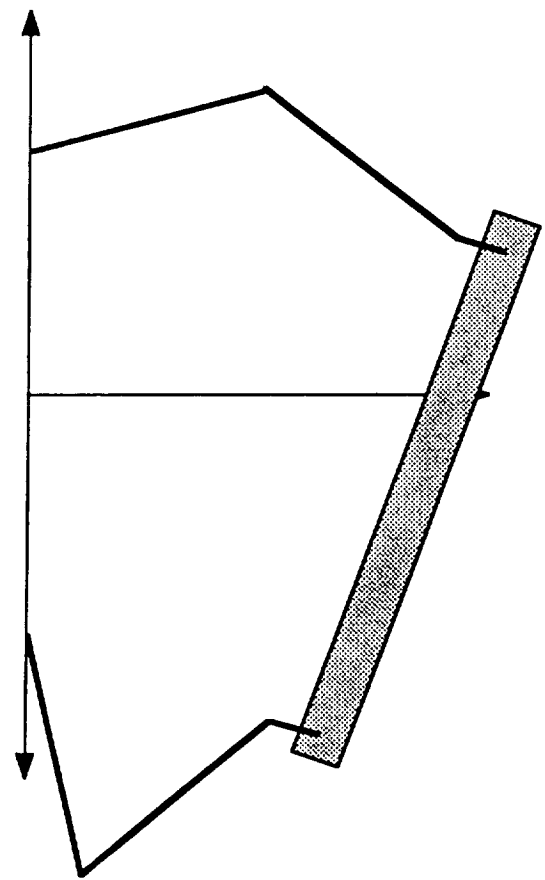


Figure 2: Free-body diagram showing interaction forces for arms grasping payload.

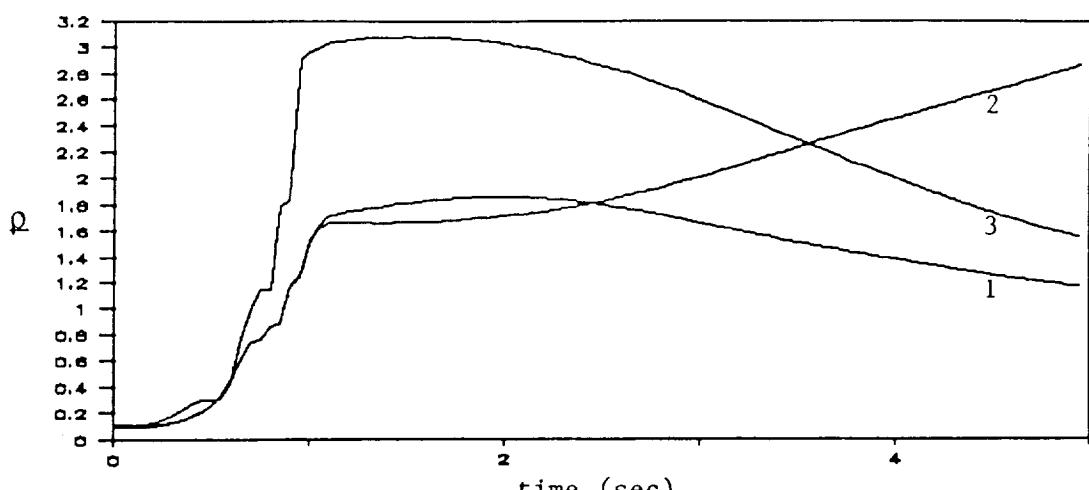


(a)

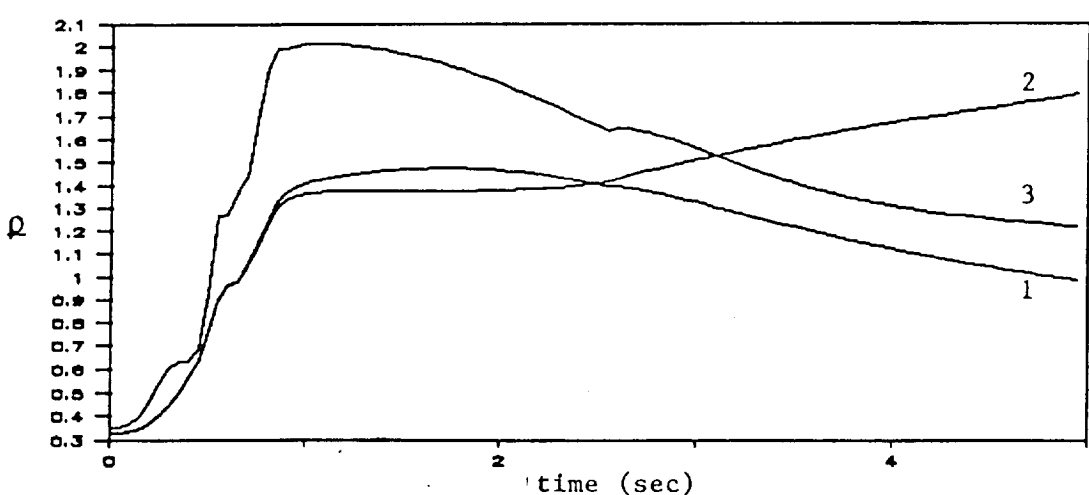


(b)

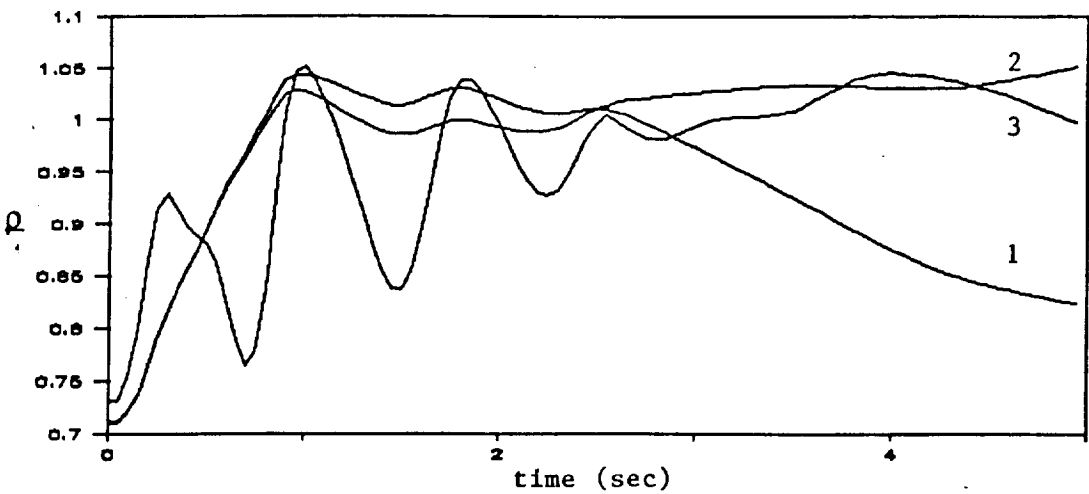
Figure 3: Initial (a) and final (b) configurations used in simulations.



(a)

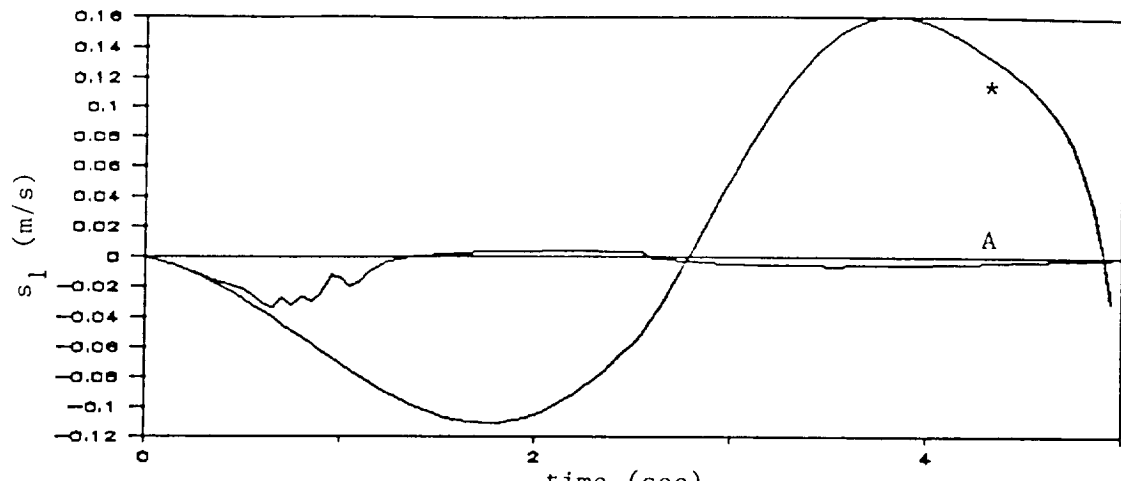


(b)

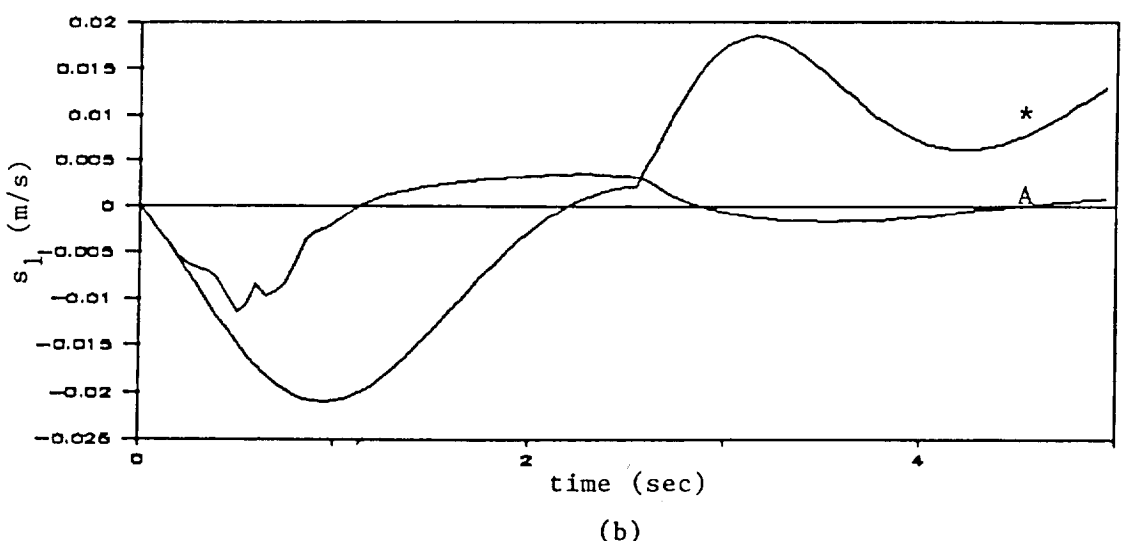


(c)

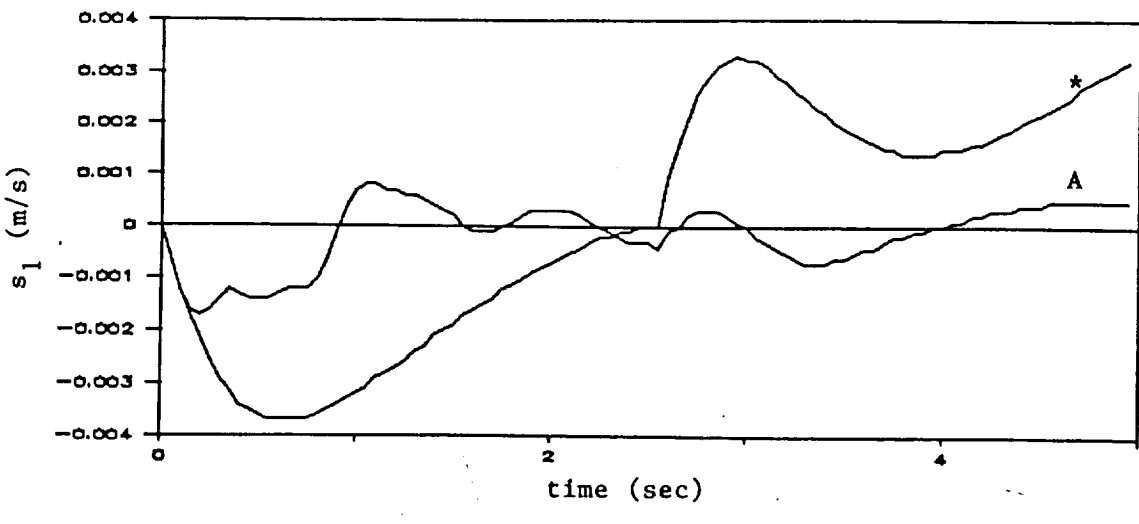
Figure 4: Normalized parameters ρ versus time for payload/arm mass-inertia ratios of (a) $1/5$, (b) 1 and (c) 5 .



(a)

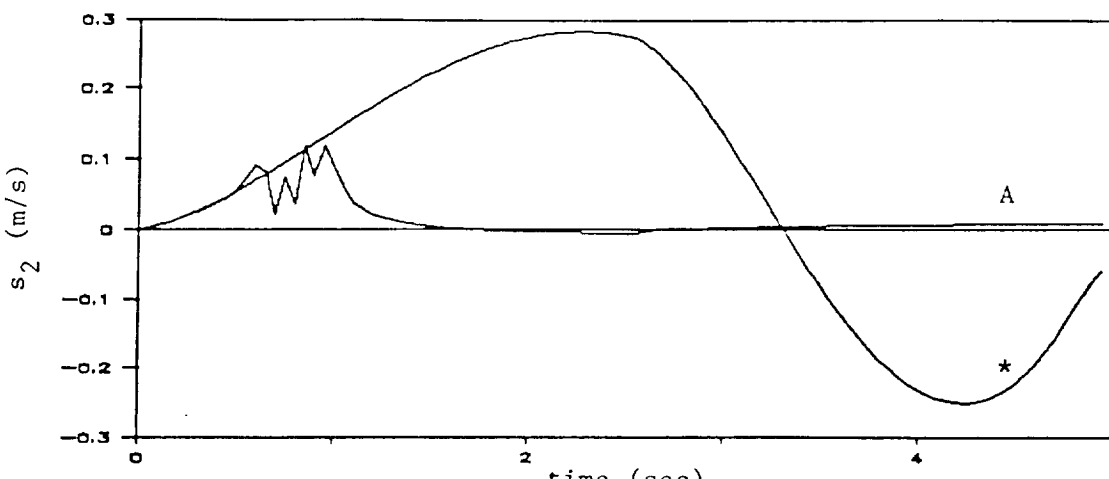


(b)

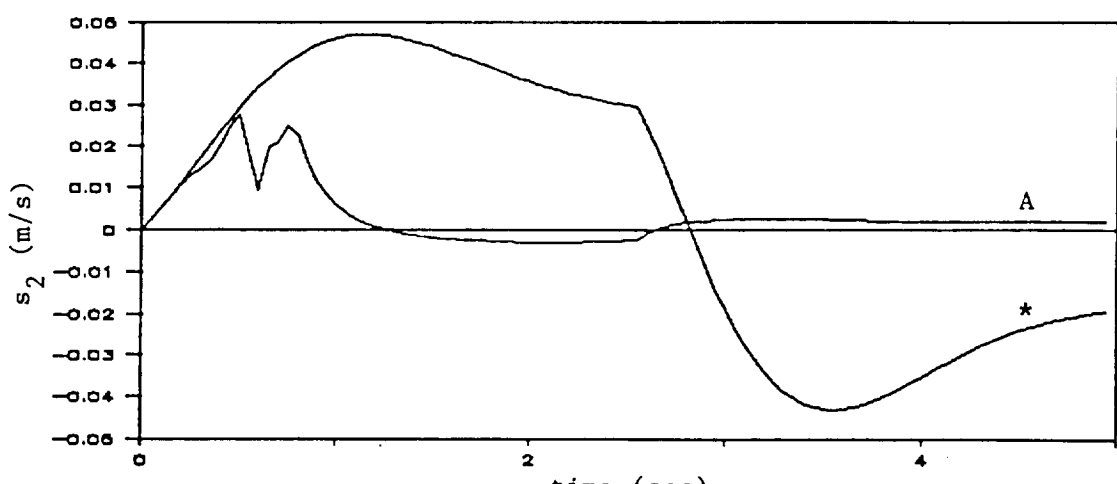


(c)

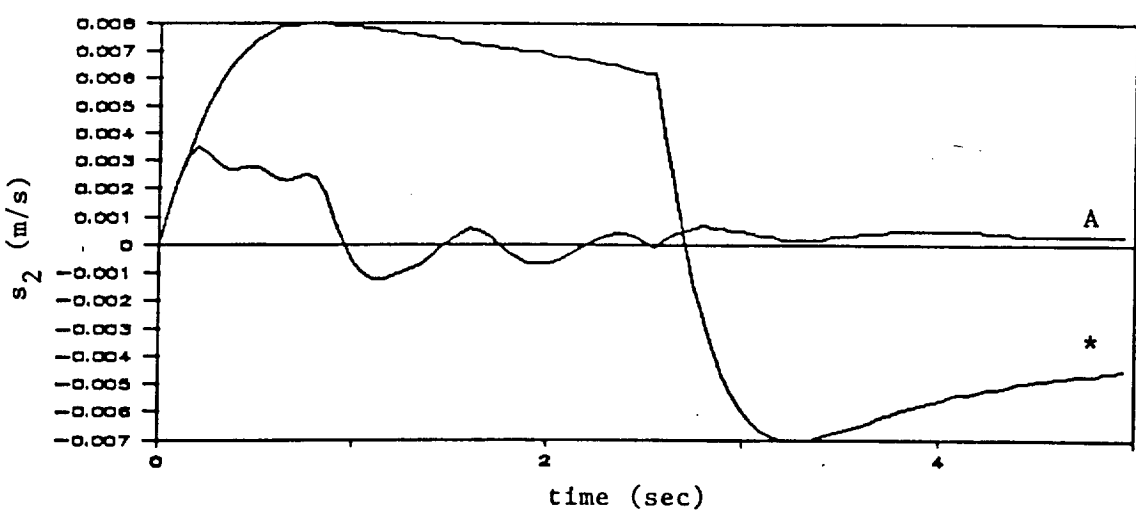
Figure 5: x_e tracking error for payload/arm mass-inertia ratios of (a) 1/5, (b) 1 and (c) 5 (parameter adaptation on (A) and off (*)).



(a)

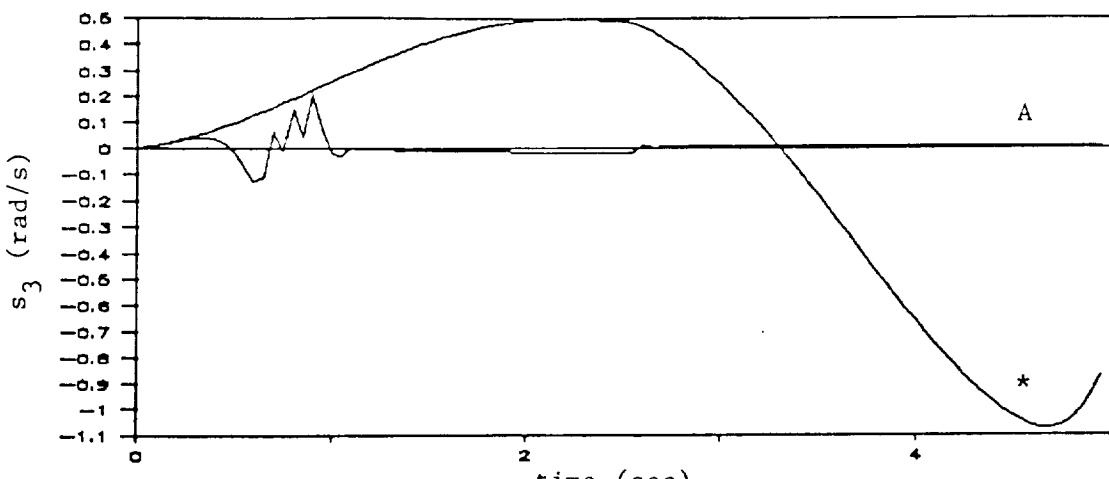


(b)

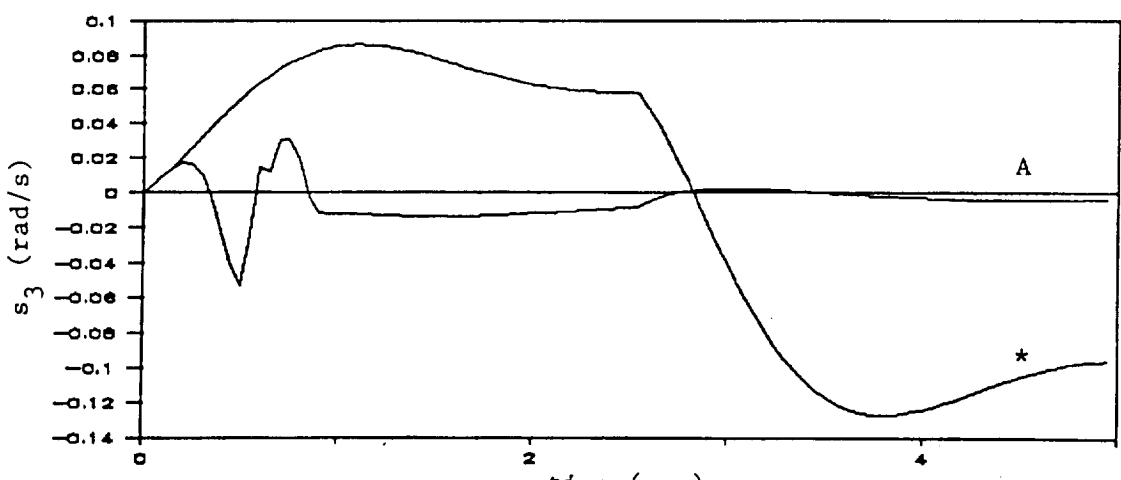


(c)

Figure 6: y_e tracking error for payload/arm mass-inertia ratios of (a) 1/5, (b) 1 and (c) 5 (parameter adaptation on (A) and off (*)).



(a)



(b)

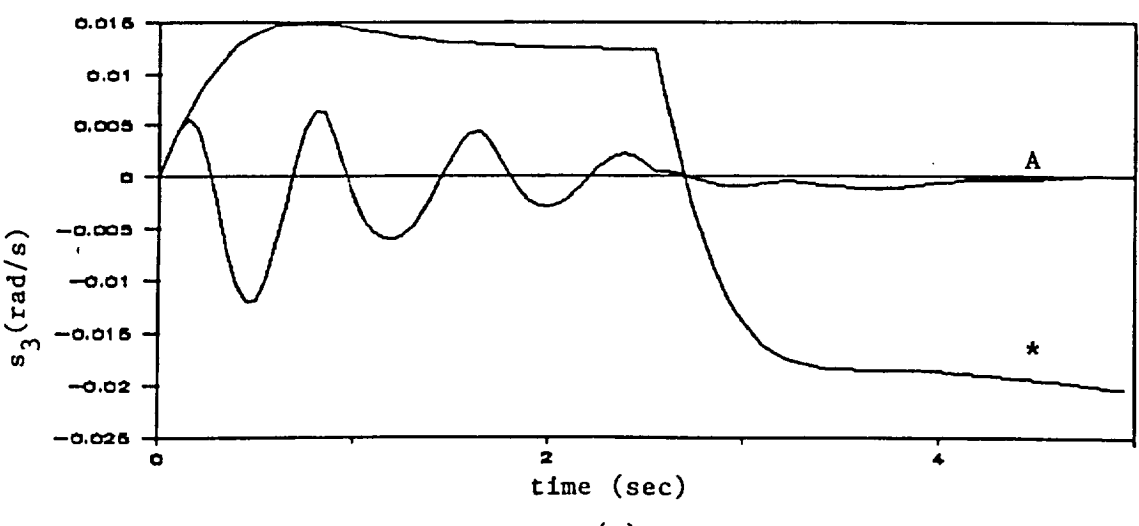


Figure 7: θ_e tracking error for payload/arm mass-inertia ratios of (a) 1/5, (b) 1 and (c) 5 (parameter adaptation on (A) and off (*)).